A Fine-Mesh Numerical Model with Detailed Boundary Layer Parameterization

Fei Jianfang (费建芳), *Zhang Ming* (张铭)
Lu Hancheng (陆汉城) and *Yang Guoxiang* (杨国祥)
Institute of Meteorology, The PLA Air Force, Nanjing 211101
Received May 15, 1991; revised April 15, 1992

ABSTRACT

A fine-mesh numerical model with thirteen-layer, three-dimensional primitive equation is designed, which has a relatively high vertical resolution in the boundary layer and detailed boundary parameterization. A strong cold frontal process is simulated by the model. Comparison of the simulated results of this process with different models shows that the result of this model is prior to that of others, and that it is necessary to increase the vertical resolution and to take account of the physical processes in the boundary layer.

1. INTRODUCTION

In order to simulate real atmospheric motion and to get high quality numerical forecast, we must increase horizontal and vertical resolutions of the model, and consider as many physical processes as possible in the model. Keyser and Anthes (1982), considering physical processes in the boundary layer including surface friction and eddy mixed process in their model, simulated a strong and narrow upward current in the vicinity of a frontal surface. Pilke (1974), using a three-dimensional primitive equation model with the detailed boundary layer parameterization, discussed the formation and development of a sea breeze front. Besides, Busch (1976), using a one-dimensional boundary layer model, studied the dynamic structure of a mesoscale system. Yamagish (1980) designed a three-dimensional model with the detailed boundary layer parameterization, simulated a transformation process of a cold air-mass affecting Japan.

If we want to consider the boundary layer physical processes in the model, and use to study the cases, the observed boundary layer data must be possessed. The dense meteorological data in time and space gained during the Mesoscale Weather Experiment over the East China supply the initial fields for us to design the fine-mesh numerical model with the detailed boundary layer parameterization, and the simulated results are compared with the observed field. In this paper a fine-mesh three- dimensional primitive equation numerical model with thirteen layers in the vertical is designed under the frame of Zhou's model (1980). This model has a relatively high vertical resolution in the boundary layer and the detailed boundary layer parameterization. And it has higher resolution than Zhou's model in the vertical, especially, in the boundary layer and the physical processes in the boundary layer is more detailedly considered.

A cold frontal process on 28 April 1983 during the Mesoscale Weather Experiment over the East China is simulated by this model. The design of the model is emphatically described in the paper. The simulated results of the cold frontal process by the model is briefly compared with results simulated by other models. The detailed simulation results of the cold frontal process is presented in another paper.

II. DESIGN OF THE MODEL

1. Governing Equations

The σ −system is used in the model, where $\sigma = \dfrac{(P - P_t)}{\pi}$, $\pi = P_s - P_t$, P_s is the surface pressure, P_t the pressure at the top of the model atmosphere. The primitive equations utilized in the model are as follows:

$$\frac{\partial}{\partial t}(\frac{\pi u}{m^2}) = -\frac{\partial}{\partial x}(\frac{\pi u^2}{m}) - \frac{\partial}{\partial y}(\frac{\pi uv}{m}) - \frac{\partial}{\partial \sigma}(\frac{\pi u\dot{\sigma}}{m^2}) + \frac{1}{m^2} f\pi v' + \frac{\pi v}{m^2}(-v\frac{\partial m}{\partial x} + u\frac{\partial m}{\partial y}) + \frac{\pi}{m^2}F_u - \frac{g}{m^2}(\frac{\partial \overrightarrow{\tau}}{\partial \sigma})_x \tag{1}$$

$$\frac{\partial}{\partial t}(\frac{\pi v}{m^2}) = -\frac{\partial}{\partial x}(\frac{\pi uv}{m}) - \frac{\partial}{\partial y}(\frac{\pi v^2}{m}) - \frac{\partial}{\partial \sigma}(\frac{\pi v\dot{\sigma}}{m^2}) + \frac{1}{m^2} f\pi u' + \frac{\pi u}{m^2}(v\frac{\partial m}{\partial x} - u\frac{\partial m}{\partial y}) + \frac{\pi}{m^2}F_v - \frac{g}{m^2}(\frac{\partial \overrightarrow{\tau}}{\partial \sigma})_y \tag{2}$$

$$\frac{\partial}{\partial t}(\frac{\pi C_p T}{m^2}) = -\frac{\partial}{\partial x}\frac{\pi}{m}(C_p T + \varphi)u - \frac{\partial}{\partial y}\frac{\pi}{m}(C_p T + \varphi)v - \frac{\partial}{\partial \sigma}\frac{\pi}{m^2}(C_p T + \varphi)\dot{\sigma} + \frac{1}{m^2}(\frac{\sigma\pi RT}{\sigma\pi + P_t} - \varphi)\frac{\partial \pi}{\partial t} + \frac{\pi}{m^2}(uf v_g - vf u_g) + \frac{C_p \pi}{m^2}F_T + \frac{L\pi}{m^2}\dot{Q} + \frac{g}{m^2}\frac{\partial H}{\partial \sigma} \tag{3}$$

$$\frac{\partial}{\partial t}(\frac{\pi q}{m^2}) = -\frac{\partial}{\partial x}(\frac{\pi qu}{m}) - \frac{\partial}{\partial y}(\frac{\pi qv}{m}) - \frac{\partial}{\partial \sigma}(\frac{\pi q\dot{\sigma}}{m^2}) + \frac{\pi}{m^2}\dot{Q} + \frac{g}{m^2}\frac{\partial E}{\partial \sigma} \tag{4}$$

$$\frac{\partial}{\partial t}(\frac{\pi}{m^2}) = -\frac{\partial}{\partial x}(\frac{\pi u}{m}) - \frac{\partial}{\partial y}(\frac{\pi v}{m}) - \frac{\partial}{\partial \sigma}(\frac{\pi\dot{\sigma}}{m^2}) \tag{5}$$

$$\frac{\partial}{\partial t}\frac{\partial \varphi}{\partial \ln(\sigma + \frac{P_t}{\pi})} = -R\frac{\partial T}{\partial t} \tag{6}$$

$$\frac{\pi\dot{\sigma}}{m^2} = \int_{\sigma_T}^{\sigma}\frac{\partial}{\partial \sigma}(\frac{\pi\dot{\sigma}}{m^2})d\sigma = -\int_{\sigma_T}^{\sigma}\frac{\partial \pi}{\partial t}d\sigma - \int_{\sigma_T}^{\sigma}[\frac{\partial}{\partial x}(\frac{\pi u}{m}) + \frac{\partial}{\partial y}(\frac{\pi v}{m})]d\sigma \tag{7}$$

where

$$fv_g = (\frac{\partial \varphi}{\partial x} + \frac{\sigma RT}{\sigma\pi + P_t}\frac{\partial \pi}{\partial x})m \tag{8}$$

$$-fu_g = (\frac{\partial \varphi}{\partial y} + \frac{\sigma RT}{\sigma\pi + P_t}\frac{\partial \pi}{\partial y})m \tag{9}$$

$$u' = u_g - u \tag{10}$$

$$v' = v_g + v \tag{11}$$

In the above equations, the symbols F_u, F_v, F_T and F_q indicate the subgrid scale horizontal diffusion terms for momentum (u and v components), heat and moisture, respectively. $\dot{Q}$ is the condensation rate of moisture, L the condensation latent heat. The horizontal stress vector ($\vec{\tau}$) due to the vertical turbulent fluxes of horizontal momentum is expressed as

$$\vec{\tau} = -\left(\frac{\rho^2}{\pi} g\right) K_m \frac{\partial \vec{V}}{\partial \sigma} \tag{12}$$

where K_m is the eddy exchange coefficient for momentum, and ρ the air density. The vertical turbulent fluxes of heat and moisture are expressed as

$$H = (C_p \rho^2 g / \pi) K_h \partial\theta / \partial\sigma \tag{13}$$

$$E = (\rho^2 g / \pi) K_h \partial q / \partial\sigma \tag{14}$$

respectively, where K_h is eddy exchange coefficient. Other notations are conventional.

2. Structure of the Model

In order to yield higher accuracy of the treatment of vertical turbulent transfer processes and to consider more properties of the boundary layer, we designed a fine-mesh numerical model which has a relatively high vertical resolution in the boundary layer.

The model has thirteen levels in the vertical (Fig.1). Vertical resolution is set relatively high in the lower model atmosphere. The top of the model atmosphere is located at 100hPa ($\sigma = 0$). Variables (u,v,T and q) are defined on the integer number levels, the eddy exchange coefficients (K_m and K_h)and $\dot{\sigma}$ on the half number levels (Fig.1). For the sake of convenience, topography is not yet considered in the model. The sea level is looked as the lower boundary.

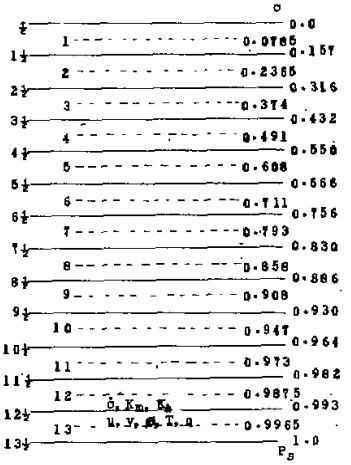

Fig. 1. Vertical grid structure of the model showing vertical indexing and levels at which various variables are defined.

3. *Space Difference and Temporal Integration Scheme*

There are only two types of the space difference in Eqs.(1)–(7). one type is $\nabla_h \cdot \pi\vec{V}A/m$, where A is any variables, $\vec{V}$ the horizontal wind vector. The other type is $\frac{\partial\varphi}{\partial x}+\frac{\sigma\pi RT}{\sigma\pi+P_t}\frac{\partial\pi}{\partial x}$, which is used to calculate geostrophic wind.

The finite-difference of the horizontal flux divergence term is expressed as

$$\nabla_h \pi\vec{V}A/m=(\overline{\pi u}^x\overline{A}^x/m)_x+(\overline{\pi v}^y\overline{A}^y/m)_y \tag{15}$$

where

$$\overline{A}^x=(A(x+\frac{\Delta x}{2})+A(x-\frac{\Delta x}{2}))/2 \tag{16}$$

$$A_{x_2}=(A(x+\frac{\Delta x}{2})-A(x-\frac{\Delta x}{2}))/2\Delta x \tag{17}$$

The finite-difference of the term $\frac{\partial\varphi}{\partial x}+\frac{\sigma\pi RT}{\sigma\pi+P_t}\frac{\partial\pi}{\partial x}$ is expressed as

$$\frac{fv_g}{m}=\frac{\partial\varphi}{\partial x}+\frac{\sigma\pi RT}{\sigma\pi+P_t}\frac{\partial\pi}{\partial x}\approx[(\varphi_{i+1,j}-\varphi_{i-1,j})+(\frac{\sigma\pi RT}{\sigma\pi+P_t})_{i,j}(\pi_{i+1,j}-\pi_{i-1,j})]/2\Delta s \tag{18}$$

where Δs is the horizontal mesh size, and $\Delta s=\Delta x=\Delta y=30km$.

In order to increase the computational accuracy of the thermal advection, the hydrostatic equation is differentiated once in the model (Zhou 1980). Its finite-difference equation is

$$\varphi_k^{n+1}=(\varphi_k^{n-1}+\varphi_{k+1}^{n+1}-\varphi_{k+1}^{n-1})-\frac{R}{2}\ln\frac{(\sigma_k+P_t/\pi)}{(\sigma_{k+1}+P_t/\pi)}(T_k^{n+1}-T_k^{n-1}+T_{k+1}^{n+1}-T_{k+1}^{n-1}) . \tag{19}$$

The form

$$\varphi_k^{n+1}=\varphi_k^{n-1}+\frac{R}{2}(T_k^{n+1}-T_k^{n-1}+T_0^{n+1}-T_0^{n-1})\ln\frac{(\sigma_k+P_t/\pi)}{(1+P_t/\pi)} \tag{20}$$

is to obtain φ at the lowest layer of the model. In (20), T_0 is the surface temperature.

The time-integration scheme utilized in the model is the scheme that combines the leap-frog method and the Euler- backward method. We use a temporal smoothing operator in the model so as to eliminate the computational mode for $2\Delta t$ period.

The model time-integration starts from 1000Z 28 April 1983. The time interval Δt is 60 seconds.

4. *Physical Processes in the Model*

(1). *Boundary layer parameterization*

It is very beneficial that the detailed physical processes in the boundary layer in the model are considered to increase the simulation and forecast abilities of the model. It is also very important for further studying the effect of the boundary layer on whole atmospheric motion.

The boundary layer is divided into the surface layer and Ekman layer in the model.

The chosen parameterization scheme for the surface fluxes (momentum, heat and moisture) is based on Monin–Obukhov similarity theory in the surface layer. A surface energy budget equation is used to predict the ground temperature. A method suggested by O'Brien (1970) is utilized to calculate vertical turbulent fluxes of momentum, heat and moisture above the surface layer.

a. *Surface fluxes*

Based on Monin–Obukhov similarity theory, we get

$$\frac{k_0 Z}{u_*}\frac{\partial \vec{V}}{\partial Z} = \varphi_m(Z/L) \tag{21}$$

$$\frac{k_0 Z}{\theta_*}\frac{\partial \theta}{\partial Z} = \varphi_h(Z/L) \tag{22}$$

$$\frac{k_0 Z}{q_*}\frac{\partial q}{\partial Z} = \varphi_q(Z/L) \tag{23}$$

where k_0 is the Von–Karman constant, and $L = T_0 u_*^2 / k_0 g\theta_*$ is the Monin–Obukhov length. The quantities u_*, θ_* and q_* are defined as, respectively

$$\tau_0 = \rho_0 \overline{|w'V'|}_0 = \rho_0 u_*^2 \tag{24}$$

$$H_0 = \rho_0 C_p \overline{(w'T')}_0 = -\rho_0 C_p u_* \theta_* \tag{25}$$

$$E_0 = \rho_0 \overline{(w'q')}_0 = -\rho_0 u_* q_* \tag{26}$$

where subscript "0" indicates the value at the earth's surface.

The values of u_*, θ_* and q_* are given by

$$u_* = k_0 |\vec{V}| / [\ln(Z/Z_0) - \psi_m(Z/L)] \tag{27}$$

$$\theta_* = k_0(\theta(Z) - \theta_{Z_0}) / 0.74[\ln(Z/Z_0) - \psi_h(Z/L)] \tag{28}$$

$$q_* = k_0(q(Z) - q_{Z_0}) / 0.74[\ln(Z/Z_0) - \psi_q(Z/L)] \tag{29}$$

where Z_0 is the roughness parameter. The height Z is located on the height of the lowest model level. We assume that the values at Z_0 are the same as those at the surface. The alternate method is used to calculate u_*, θ_* and q_*. The calculation marches forward in the following way: First, an initial guess of L is estimated from the values of u_* and θ_* at time $t - \Delta t$. This value of L is used in (27) and (28) to estimate u_0, and θ_0 at time t, which are then used to calculate an update value of L. This alternate procedure continues until the solution converges.

An energy budget equation is utilized to forecast the ground temperature:

$$C_g \frac{\partial \theta_0}{\partial t} = R_n - H_m - H_g - E \tag{30}$$

where C_g is the thermal capacity of the slab per unit area. The terms on the right-hand side

of (30) are described as follows (Zhang,1982; Wu et al.,1984):

(a). *Radiative flux* (R_n)

Radiation is the basic driving force of the planetary boundary layer and the most important component of the ground energy budget. R_n is expressed as:

$$R_n = Q_s + I\downarrow - I\uparrow \tag{31}$$

where Q_s is the amount of solar radiation absorbed by the ground. Q_s is approximated as

$$Q_s = S(1 - A)(\cos\xi)\tau_s^{\sec\zeta} \tag{32}$$

where s denotes the intensity of solar radiation at the top of the atmosphere, A the albedo, ζ the solar zenith angle, τ_s the atmospheric transmissivity, and

$$\cos\zeta = \sin\varphi\sin\delta - \cos\varphi\cos\delta\cos h \tag{33}$$

in which φ represents the latitude, δ the solar declination, and $\delta = 23.5\sin\frac{\pi}{365}(T - 81.5)$, h the local angle of the sun.

In (31), $I\downarrow$ denotes the incoming of the net longwave radiation, and it is a constant. $I\uparrow$ is the outgoing of the net longwave radiation:

$$I\uparrow = \varepsilon\sigma_s T_g^4 \tag{34}$$

where ε is the ground emissivity (0.9–1.0), σ_s the Stefan–Boltzmann constant.

(b). *Transfer of heat due to molecular conduction between the surface and the soil* (H_m)

The transfer of heat due to molecular conduction between the surface and the soil is calculated from the equation:

$$H_m = K_m C_g(T_0 - \overline{T}_m) \tag{35}$$

where K_m is the heat transfer coefficient expressed as $K_m = 1.18\omega$ (ω is the angular velocity of the earth), $\overline{T}_m$ is taken to be equal to the mean surface air temperature over the previous 24h.

(c). *Sensible heat exchange between the ground and the air* (H_g)

The flux of sensible heat due to the combined molecular conduction and turbulent transfer is given as

$$H_g = K_s C_g(T_0 - T_Z) \tag{36}$$

where K_s is the heat transfer coefficient, and $K_s = \omega + K'_s u_*$, T_Z is the temperature of the lowest model level. A constant value of K'_s is assumed for $3 \times 10^{-3}\mathrm{m}^{-1}$.

(d). *Latent heat exchange of the ground and the air* (E)

The latent heat exchange of the ground and the air is expressed as

$$E = L\rho_0\overline{w'q'} = -L\rho_0 u_* q_* \tag{37}$$

Table 1 gives the units and value of the variables which are used in the surface energy budget equation.

b. *Eddy fluxes of momentum, heat and moisture above surface layer*

The vertical turbulent exchange coefficients of momentum, heat and moisture suggested by O'Brien(1970) are expressed as

$$K_\eta(Z)=\begin{cases} K_\eta|_H+[(H-Z)^2/(H-h)^2]\times\{K_\eta|_h-K_\eta|_H+(Z-h)\times \\ \left[\left.\frac{\partial K_\eta}{\partial Z}\right|_h+2(K_\eta|_h-K_\eta|_H)/(H-h)\right]\} & h\leqslant Z\leqslant H \\ K_\eta|_h & Z>H \\ (Z/h)\,K_\eta|_h & Z<h \end{cases} \tag{38}$$

where the subscript η indicates the turbulent exchange coefficient of momentum , heat and moisture , H is the height of the boundary layer top, h the height of the surface layer top. We assume that $K_\eta|_H$ is very small, $K_\eta|_H\sim10^{-4}$. Therefore, the vertical turbulent terms of momentum, heat and moisture are expressed as

$$(\frac{\vec{\tau}}{\rho})_x=-\overline{u'w'}=K_m\frac{\partial u}{\partial Z} \tag{39}$$

$$(\frac{\vec{\tau}}{\rho})_y=-\overline{v'w'}=K_m\frac{\partial v}{\partial Z} \tag{40}$$

$$\frac{H}{\rho C_p}=\overline{T'w'}=K_h\frac{\partial\theta}{\partial Z} \tag{41}$$

$$\frac{E}{\rho}=\overline{q'w'}=-K_h\frac{\partial q}{\partial Z} \tag{42}$$

The top of the planetary boundary layer is located on the inversion lid of front in the model. If there is no frontal inversion, it is located on the 8th level of the model. The height of the lowest model level is defined as the top of the model surface layer.

Table 1. Value of Constants Used in the Model

S	1370 J m^{-2} s^{-1}	K'_s	3×10^{-3}m^{-1}
I$\downarrow$	275 J m^{-2} s^{-1}	C_g	8×10^4 J m^{-2} K^{-1}
τ_s	0.9	A	0.2
σ_s	5.6703×10^{-8} J m^{-2} K^{-4} s^{-1}	Z_0	0.04m
ω	7.27×10^{-5} s^{-1}		

(2). *Precipitation processes*

Precipitation processes considered in this model include large scale and cumulus convective precipitation. A method of saturated condensation is used to calculate large scale precipitation. The chosen parameterization scheme for cumulus convective precipitation is based on the scheme suggested by Kuo(1965).

(3). *Horizontal eddy diffusion*

The horizontal eddy diffusion terms of momentum, heat and moisture are expressed as

$$\pi F_\alpha = \pi A_\alpha \nabla^2 \alpha \qquad \alpha = u, v, T, q \tag{43}$$

where A_α is the horizontal eddy diffusion coefficient of momentum (heat or moisture), which is taken as a constant, and A = 1.5 $m^2 s^{-1}$.

5. *Initial Field and Lateral Boundary Condition*

The denser meteorological data in time and space were gained during the Mesoscale Weather Experiment over the East China. A strong frontal process observed on 28 April 1983 during the experiment is regarded as the initial field of the model. We obtain the initial field data on the fine-mesh size of 30 km by linear interpolation of the manually analyzed field on the grid net with mech size of 90 km.

The sponge boundary condition is utilized as the horizontal lateral boundary condition so as to eliminate computational noise.

III. COMPARISON OF MODELS

A cold frontal process on 28 April 1983 is simulated by the above described model as well as a five-layer in the vertical, fine-mesh numerical model designed by Zhou (1980). Zhou's model uses σ -system, too. The highest layer of Zhou's model is located on 200 hPa. Large scale and cumulus convective precipitation, action of frictional stress only on the lowest layer of the model are considered in his model. Besides, we change it into a model with equal interval thirteen levels in vertical that has the same physical processes as the five layer model. But, action of friction stress is considered on the lowest three layers.

For the sake of convenience, the five-layer,equal and unequal interval thirteen-level models are called A, B and C model, respectively.

Fig.2(a,b,c,d) shows the observed and simulated 1000hPa temperature fields at 1600Z 28 April, 1983.

Table 2 shows the observed and the simulated mean horizontal temperature gradients in frontal zone (i.e., horizontal temperature gradient in south-north direction for east-west direction 10 grid points' mean temperature in west frontal zone) and the maximum horizontal temperature gradients (i.e., a maximum value of south-north direction horizontal temperature gradient for the 10 grid points in west frontal zone).

Table 2. Models' and Observed Mean and Maximum Horizontal Temperature Gradients in Frontal Zone. *Unit: ℃ / 30 km*

	$-\overline{(\frac{\partial T}{\partial y})}$	$-(\frac{\partial T}{\partial y})_{max}$
A model	1.35	2.0
B model	2.0	3.2
C model	2.9	3.4
the observed	4.0	-

The thermo-isopleths of the observed temperature field shows wavelike distributionafter the cold front (Fig.2a). The horizontal temperature gradient in the east frontal zone is obviously smaller than in the west. From the simulated results of C model (Fig.2b), stronger cold air is located on the west section of forecast region, and the strength of the west frontal zone is stronger than the east. This is roughly consistent with the observed field, and the location of the frontal surface is approximately the same as the observed. The simulated result of A model or B model is not as good as that of C model. For instance, the temperature field simulated by A or B model does not reflect that the strength of the west cold front is stronger than that of the east; the velocity of the eastern cold front is too faster. Moreover, the strength of warm and cold air simulated by C model is approximately the same as the observed, but the strength by A or B model is weaker than the observed especially by A model.

Through above analyses and comparisons, we find that the strength of cold front simulated by those three models is weaker than the observed. The reasons may be as follows: one is that horizontal temperature gradient is homogenized because of smoothing initial fields and horizontal difference, the other is that the fixed lateral boundary condition is used so that the north cold air does not advect to the forecast domain. The observed situation of wavelike thermo-isopleths after the cold front is not reflected in those models, because the relief with detaining action is not considered.

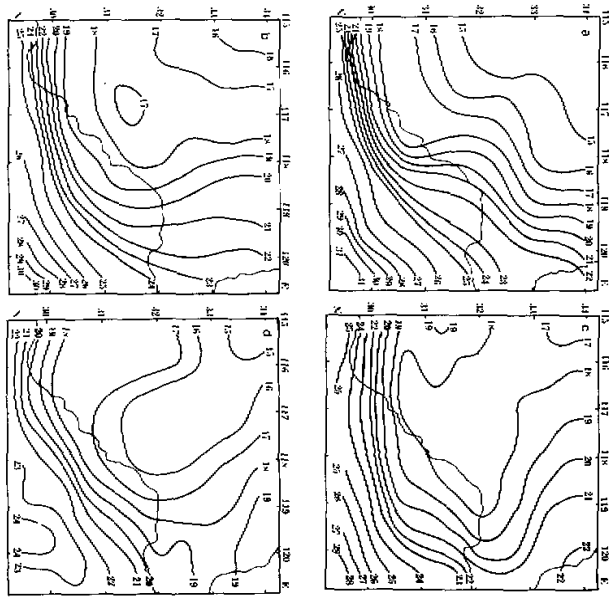

Fig.2. 1000 hPa temperature field at 1600Z 28 April, 1983.a. the observed b. Cmodel c. Bmodel d. model.

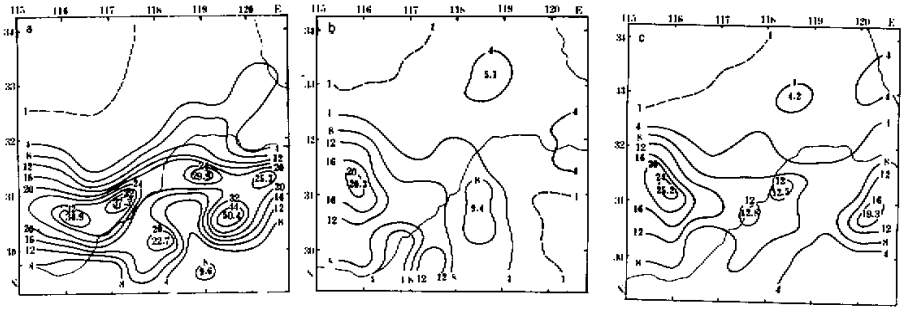

Fig.3. 9hs precipitation (from 1000Z to 1900Z). Unit: mm.a. the observed b. B model c. C model.

Though comparisons of the results of those three models, we see that the strength of cold front simulated by A, B and C models are not same. This relates probably to vertical resolution and the boundary layer processes. The strength of the cold front by C model is relatively close to the observed. There are two important reasons. First, vertical resolution of C model in the PBL is increased so that truncation error due to vertical difference in the boundary layer is decreased. Second, detailed boundary layer physical processes are considered, meanwhile, vertical eddy exchange coefficients varying with height are used, consequently, eddy transportation of physical variables in vertical can be really simulated.

Fig.3(a,b,c) shows the observed and B, C model simulated 9h precipitation (from 1000Z to 1900Z, 28 April). The observed and C model simulated precipitations are centered on southern forecast region, but the simulated precipitation is smaller than the observed. Distribution of the observed precipitation is obviously inhomogeneous. There are six precipitation centers that show beltlike distribution except two southern precipitation centers. Precipitation area of C model also shows beltlike distribution, but has larger width than the observed. Strength of precipitation over western area is close to the observed.

Comparing the results of B and C models, we find that the simulated precipitations in the vicinity of western boundary are comparatively identical, but there are larger differnce in other areas. For example, there is a 19.3 mm precipitation center for C model over the eastern area, which is comparatively consistent with the observed, but there is only 7.0 mm precipitation center for B model in the vicinity of eastern boubdary and its location over the north. Besides, the position of two precipitation centers simulated by C model in the center area is approximately the same as the observed, but for B model, there is a 9.4 mm precipitation center with its position over south, range of the precipitation is larger than the observed.

The strength and distribution of 9 h precipitation simulated by A model is more different from the observed (figure not shown).

According to evolution of the cold frontal precipitation process, the observed maximum

precipitation of 11.8 mm for 3 h (from 0700Z to 1000Z, 28 April) is located at the central section of simulated region (near Dingyun, Anhui Province). In addition, a weaker precipitation of 2.6 mm is located at north-west direction of Huoshan (figure not shown).The observed precipitation figure for 9 h (from 1000Z to 1900Z) obviously shows these two precipitation areas which move southward slightly. Distribution of the simulation precipitation by C model for 9 h is roughly the same as the observed. The simulation result of C model really shows the precipitation situation of the cold frontal process.

Some differences of strength and position of precipitation between C model and the observed are mainly because that topography is not considered in the model. It is located over the mountain area that precipitation centers are simulated not well (for example, precipitation center of 22.7 mm near Huanshan mountain is not simulated). The effect of frictional convergence and forced lifting by topography may enhance precipitation strength.

IV. CONCLUSION

A fine-mesh numerical model is designed, which has a relatively high vertical resolution in the boundary layer and detailed boundary layer parameterization. A strong cold frontal process is successfully simulated by the model. This model keeps steady when it is integrated for 18 h. In this paper, precious 9 h simulation results are given because data of the Mesoscale Weather Experiment over East China are used for the initial field, simulation area is too small and the cold front moves out of the forecast region, later the simulated results have no significance. It is neccessary to enlarge simulation region for getting a whole weather process.

In order to verify the properties of the model, comparisons of the different models' simulation results of the cold frontal process show that the simulated results of C model is superior to those of others, and it is necessary to increase the vertical resolution, especially in the boundary layer, and to take account of the physical processes in the boundary layer. Of course, it is necessary that this model is compared with other models and more weather processes are simulated by this model.

It is very important that the topography is considered in the model, this is the further work for us.

REFERENCES

Busch N. E. (1976), A multi-level model of the planetary boundary layer suitable for use with mesoscale dynamic model, *J. Appl. Meteor.*, **15**: 909-919.

Keyser D. and Anthes R. A. (1982), *Influence of planetary boundary layer on frontal structure in the* Hoskins-Bretherton horizontal shear model, *J. Atmos. Sci.*, **39**: 1782-1802.

Kuo H. L. (1965), On formation and intensification of tropical cyclones through latent heat release by cumulus convection, *J. Atmos. Sci.*, **22**: 40-63.

O'Brien J. J. (1970), A note on the vertical structure of the eddy exchange coefficient in the planetary boundary layer, *J. Atmos. Sci.*, **27**: 1213-1215.

Pielke R. A. (1974), A three dimensional numerical model of the sea breeze over South Florida, *J. Atmos. Sci.*, **102**: 115-139.

Wu Huiding and Zhang Xingwang (1984), A numerical model of atmospheric boundary layer, *Acta. Meteor. Sinica*, **42**: 290–300 (in Chinese with English abstract).

Yamagishi Y. (1980), Simulation of the air–mass transformation process using a numerical model with the detailed boundary layer parmeterization, *J. Meteor. Soc. Japan*, **58**: 357–377.

Zhang D.–L. (1982), A high–resolution model of the planetary boundary layer–sensitivity tests and comparisons with SESAME–79 data, *J. Appl. Meteor.*, **21**: 1594–1609.

Zhou Xiaoping (1980), An introduction of a fine–mesh numerical weather model, Institute of Atmospheric Physics, Academia Sinica (in Chinese).